Direct Measurement of Energetic Electrons Coupling to an Imploding Low-Adiabat Inertial Confinement Fusion Capsule

T. Döppner,[1] C. A. Thomas,[1] L. Divol,[1] E. L. Dewald,[1] P. M. Celliers,[1] D. K. Bradley,[1] D. A. Callahan,[1] S. N. Dixit,[1] J. A. Harte,[1] S. M. Glenn,[1] S. W. Haan,[1] N. Izumi,[1] G. A. Kyrala,[2] G. LaCaille,[1] J. K. Kline,[2] W. L. Kruer,[1] T. Ma,[1] A. J. MacKinnon,[1] J. M. McNaney,[1] N. B. Meezan,[1] H. F. Robey,[1] J. D. Salmonson,[1] L. J. Suter,[1] G. B. Zimmerman,[1] M. J. Edwards,[1] B. J. MacGowan,[1] J. D. Kilkenny,[3] J. D. Lindl,[1] B. M. Van Wonterghem,[1] L. J. Atherton,[1] E. I. Moses,[1] S. H. Glenzer,[1] and O. L. Landen[1]

[1]*Lawrence Livermore National Laboratory, Livermore, California 94550, USA*
[2]*Los Alamos National Laboratory, Los Alamos, New Mexico 87545, USA*
[3]*General Atomics, San Diego, California 92121, USA*

(Received 26 November 2011; published 30 March 2012)

We have imaged hard x-ray (> 100 keV) bremsstrahlung emission from energetic electrons slowing in a plastic ablator shell during indirectly driven implosions at the National Ignition Facility. We measure 570 J in electrons with $E > 100$ keV impinging on the fusion capsule under ignition drive conditions. This translates into an acceptable increase in the adiabat α, defined as the ratio of total deuterium-tritium fuel pressure to Fermi pressure, of 3.5%. The hard x-ray observables are consistent with detailed radiative-hydrodynamics simulations, including the sourcing and transport of these high energy electrons.

DOI: 10.1103/PhysRevLett.108.135006 PACS numbers: 52.57.Fg, 52.50.Jm, 87.59.−e

Inertial confinement fusion implosion experiments compress a deuterium-tritium (DT) ice fuel layer inside a low-Z ablator capsule shell. For a given driver, keeping the DT fuel entropy low (i.e., solid DT near Fermi degeneracy) is crucial for obtaining high areal densities [1–3] to achieve central hot spot ignition and the launch of a self-sustaining burn wave into the compressed fuel. Current experiments [4] of the National Ignition Campaign (NIC) [5] use laser-heated high-Z hohlraums to indirectly drive such low entropy implosions by launching four precisely timed shock waves. One possible obstacle to high compression is the preheat of the DT by energetic electrons [6,7] produced during laser-plasma interaction (LPI) inside the hohlraum [8,9]. The resulting increase in adiabat has to remain small relative to the adiabat $\alpha = 1.5$ of the dense DT fuel after shock compression.

In this Letter, we report on the first direct measurements of the energy deposited into a plastic (CH) capsule ablator by energetic electrons in an ignition hohlraum, which allows us to infer an upper bound on the DT fuel preheat in current NIC experiments. This is achieved by imaging the bremsstrahlung emission from the capsule at energies around 115 keV through the hohlraum laser entrance hole (LEH), cf. Fig. 1. To avoid the neutron background associated with high-yield implosions, we used a surrogate capsule where the DT ice layer is replaced by an equivalent mass of CH, resulting in a ~5% thicker ablator shell. Since the outer ablator design remains unchanged, this yields the same implosion dynamics as for an ignition capsule up until approaching maximum convergence.

The hard x-ray images of the implosion experiment are complemented by spectrally and time-resolved measurements of the total hard x-ray emission from the hohlraum. A simple formula, balancing bremsstrahlung emission and stopping power for energetic electrons, is used to relate the bremsstrahlung emission I_{Br} to the amount of energetic electrons [10,11]:

$$I_{\mathrm{Br}}\left(\frac{\mathrm{keV}}{\mathrm{keV\,sr}}\right) = \frac{6.3}{4\pi} \times 10^9 Z^* E_{\mathrm{hot}}(\mathrm{J}) e^{1-h\nu/kT_{\mathrm{hot}}}, \quad (1)$$

with $Z^* = \langle Z^2 \rangle / \langle Z \rangle$ the average atomic number, E_{hot} the energy in energetic electrons, and T_{hot} the characteristic temperature of the hot electron distribution. I_{Br} scales linearly with Z, since the bremsstrahlung efficiency scales

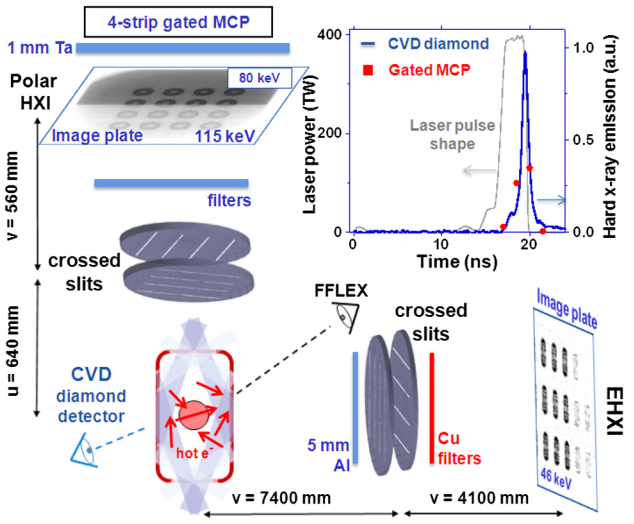

FIG. 1 (color online). Diagnostic configuration to measure spatially resolved polar and equatorial hard x-ray (> 100 keV) emission from indirectly driven fusion experiments on the NIF, which is primarily generated at the end of the laser drive.

as Z^2, while the electron stopping power scales as Z. By applying Eq. (1), we measure 570 ± 250 J of energetic electrons coupling to the CH ablator, which we find to be consistent with more detailed calculations for stopping and bremsstrahlung [12]. Consistency of experimental images with simulations further suggests that diffusion is a reasonable transport model, and, in particular, there is no evidence for anomalous transport of hot electrons to the capsule.

Figure 1 shows a schematic of the experimental configuration. We are heating a cylindrical gold hohlraum (5.44 mm diameter, 10.0 mm height, 30 μm wall thickness, filled with 359 Torr of helium at 24 K) with 192 laser beams delivering a total of 1.3 MJ at 351 nm in a 20 ns long, shaped laser pulse. The laser energy is converted to a thermal x-ray drive that reaches a peak internal temperature of 300 eV [4]. The x rays ablate the outer layers of a 2.22 mm diameter capsule with a 203 μm thick, Ge-doped CH shell that is placed at the center of the hohlraum [13]. Here, we used a surrogate capsule where the 68 μm thick DT ice layer is replaced by a 13 μm CH layer, so that the mass being accelerated is maintained [14]. The capsule is filled with a D^3He gas mixture at mass density of 8.3 mg/cm^3. As a result of the rocketlike acceleration, the capsule converges in a nearly symmetric implosion to a radius of 50 μm, as measured from time-resolved x-ray self-emission at ~9 keV [14]. In this study, we image the hard x-ray emission (> 100 keV) from the CH ablator shell that occurs before the capsule has compressed to a radius of $r \sim 0.5$ mm. Combined with a measurement of the bremsstrahlung spectrum, this provides a direct measure of the energy locally deposited into the capsule by energetic electrons using Eq. (1).

For this purpose, two time-integrating multipinhole hard x-ray imagers (HXIs) were fielded along the two principal axes of the hohlraum. The polar-view HXI (200×200 μm^2 pinholes at 640 mm from the target; magnification $M = 0.89$, with 425 μm spatial resolution) looks directly at the capsule through the LEH. The equatorial view is recorded by EHXI (250×250 μm^2 pinholes at 7.43 m from the target; magnification $M = 0.53$, with 725 μm spatial resolution). In both imagers, we utilize crossing slits machined in two 2.5 mm thick tungsten substrates to form high aspect ratio pinholes that are necessary to obtain a sufficiently high signal over background. We use imaging plate detectors (Fuji BAS-MS) with absolutely calibrated photo-stimulated luminescence (PSL) and fading characteristics [15] to record time-integrated images. The spectral sensitivity of the polar HXI peaks at 80 and 115 keV by filtering with 1.25 mm Cu and an additional 0.5 mm Ag, respectively. EHXI has three channels, centered at 46 keV (5 mm Kapton + 5 mm Al), 70 keV (additional 0.8 mm Cu filter), and 100 keV (additional 2.4 mm Cu).

Low energy electrons are completely stopped in the ablator, while electrons with high energies have the potential to traverse both the ablator and the fuel. As a measure of electrons that are able to get to the DT fuel and cause preheat, we focus on electrons with $E > 100$ keV. Figure 2 shows a polar image of the hohlraum measured by the 115 keV channel of the polar HXI, averaged over 8 individual images to improve signal to noise. It provides a direct, unattenuated view of the capsule at the center of the hohlraum. The image indicates the locations of the inner hohlraum wall, the LEH ($d_0 = 3.1$ mm), and the outer capsule diameter before the experiment. Figure 3 shows the azimuthally averaged radial lineout (shaded profile). The dominant signal clearly comes from electrons that are stopped in gold. The increased emission just inside the inner hohlraum wall is due to integration along the full hohlraum height. There is also a distinct shelf originating from the Au end cap around the LEH. The signal in the center at radii <1 mm is accounted to emission from the capsule and ablator blowoff along the line of sight.

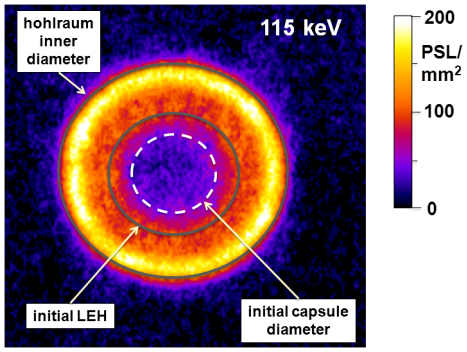

FIG. 2 (color online). Bremsstrahlung emission around 115 keV measured by the polar HXI, looking directly at the imploding capsule through the LEH of the hohlraum. The emission relates directly to energy locally deposited by energetic electrons.

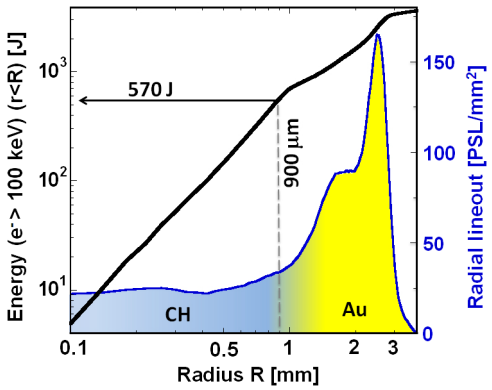

FIG. 3 (color online). By radially integrating (thick solid line) the azimuthally averaged x-ray emission (shaded profile) in the 115 keV polar HXI image, we obtain the energy deposited by electrons with $E > 100$ keV in the CH capsule shell and ablated material. Color shading indicates the transition from electrons stopping in plastic to stopping in Au at $R > 1.32$ mm.

To quantify the coupling of energetic electrons with the ablator, we have to consider a transition from stopping purely in CH at the center of the hohlraum to an interaction exclusively with gold towards the wall of the hohlraum. Time-integrated soft x-ray images measure the LEH closure [16], with the radius reduced to 1.32 mm at the end of the laser pulse due to gold ablated from the Au end cap. For our analysis, we assume a transition from CH to Au over our instrument resolution (425 μm) from 1.12 to 1.55 mm (cf. Figure 3). Note that, according to Eq. (1), ~15 times more electrons are necessary to yield the same bremsstrahlung emission from stopping in CH ($Z^* = 5.3$) compared to stopping in Au ($Z = 79$).

In addition to the spatially integrated HXI signals, we use the filter-fluorescer experiment diagnostic (FFLEX) [17] to characterize the time-integrated hard x-ray emission from the hohlraum. It consists of 10 time-integrating channels with spectral sensitivities ranging from 20 to 300 keV and provides an absolutely calibrated measurement of the total emitted hard x-ray spectrum as seen from an equatorial view with the same line of sight as EHXI. Figure 4 shows the best fit to the 16 diagnostic channels, and one can use Eq. (1) to infer the total hot electron distribution in the hohlraum. The two-temperature distribution is typical for gas-filled hohlraum experiments on the National Ignition Facility (NIF), with the lower temperature component corresponding to energetic electrons generated by stimulated Raman scattering (SRS) [18,19] ($T_1 = 18$ keV, $E_1 = 50 \pm 20$ kJ) and a hot component likely due to interaction around quarter-critical density ($T_2 = 110$ keV, $E_2 = 1.0 \pm 0.3$ kJ). The best fit includes Au K-α line emission at 67 and 69 keV, which is 8.5 times higher than the continuum. The highest energy point at 300 keV for polar HXI is derived from the enhanced background that is transmitted through individual slits, i.e., through 2.5 rather than 5 mm tungsten. For each diagnostic, images are scaled to the same gray scale for direct comparison.

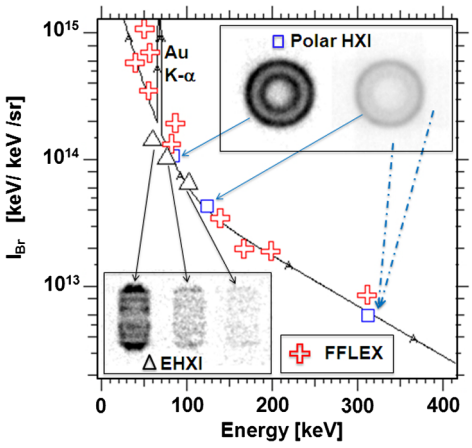

FIG. 4 (color online). Time-integrated two-temperature hard x-ray spectrum as measured by FFLEX, EHXI, and polar HXI. The best fit is obtained for $T_1 = 18$ keV ($E_1 = 50$ kJ) and $T_2 = 110$ keV ($E_2 = 1.0$ kJ).

Knowing the materials in the line of sight and the energy spectrum of hot electrons, one can calculate the total hot electron energy deposited in the capsule by combining Eq. (1) and Fig. 2. Figure 3 shows the integrated energies of electrons >100 keV ($E_{\mathrm{el}}^{>100\,\mathrm{keV}}$) required to generate the signal contained within a radius R. This was calculated by assuming that the spectrum measured in Fig. 4 is uniform in the hohlraum and thus representative of the energy spectrum stopping in the capsule. In addition, we took into account that the capsule emission is not attenuated by the 80 μm thick Au end cap (a correction by a factor of 1.7 around 100 keV) and does not contain Au K-α photons (a 20% correction).

The time history of hard x-ray emission centered at ~150 keV, as recorded by a chemical-vapor-deposited (CVD) diamond photoconductive x-ray detector and a gated four-strip multichannel plate (MCP) behind the polar HXI, shows that the majority of hot electron generation occurs close to the end of the laser pulse, cf. the inset of Fig. 1. At this time (19 ns), the capsule has compressed to a radius of 700 μm. For a conservative estimate, we add half a resolution element and consider the integrated signal up to a radius of 900 μm for further analysis. We infer 570 ± 250 J in electrons with energies >100 keV that are stopping in either the CH capsule shell or ablated mass in the same line of sight. Fully integrated simulations of the experiment that model the coupling with, stopping in, and propagation through the ablator of these energetic electrons, and subsequent stopping and heating in the DT fuel, show that less than 2% of the energy $E_{\mathrm{el}}^{>100\,\mathrm{keV}}$ absorbed in the CH ablator is absorbed in the DT ice. For better accuracy, we calculated through 1D simulations the branching ratio of electron energy deposited in the CH ablator to DT fuel as a function of electron initial energy. Convolving this with the inferred hot electron distribution shown in Fig. 4 and correcting for 2D line-of-sight effects, we derive an upper bound of energy that is absorbed in the DT ice (preheat) of 5 ± 3 J.

To estimate the effect on compressibility, this energy needs to be compared to the total internal energy in the fuel. At 19 ns, the 4 successive shocks have merged, and the 0.17 mg of DT fuel is compressed to at least 2.5 g/cc, yielding 100 J for the internal energy of the Fermi degenerate system [20]. With the adiabat $\alpha \approx 1.5$ in current NIC implosions, this allows us to infer an adiabat increase of $\delta\alpha = 0.033 \pm 0.017$ due to hot electron preheat, which is acceptable within the current error budget roll-up. We emphasize that we conducted a conservative derivation that yields an upper bound for the preheat of the DT fuel. For instance, according to simulations, up to 10% of the x-ray emission could originate from He plasma or Au blowoff at the LEH along the line of sight of the capsule.

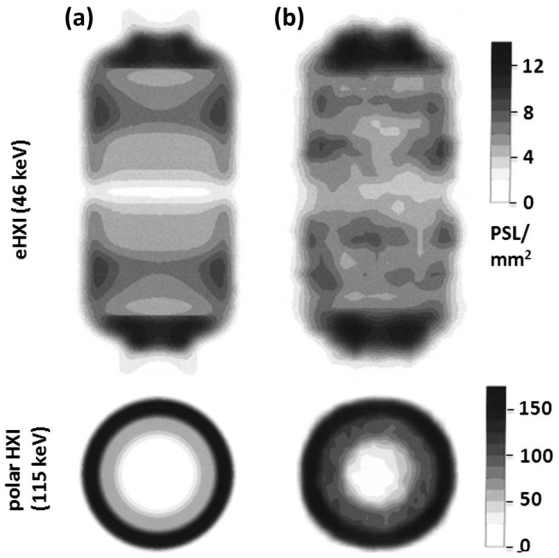

FIG. 5. (a) Synthetic images from integrated simulations reproduce the main features of (b) measured hard x-ray images along the two principal axes of the hohlraum. Bremsstrahlung generated from the stopping of energetic electrons is the dominant source of hard x-ray emission.

2D (axisymmetric) integrated simulations, including a suprathermal electron package [21] that allows for the isotropic sourcing, transport, and scatter of energetic electrons in LASNEX [22], compare well with the above analysis. Scattering and stopping formulas are consistent with the best available in the literature [23], and energy deposition was benchmarked against Monte Carlo simulation using the Integrated Tiger Series (ITS) package [24]. Bremsstrahlung emission is calculated following the parametrization found in Ref. [25], and ionization effects are included throughout.

The sourcing of energetic electrons in time and space relies on LPI considerations inferred from backscatter [26] and hard x-ray measurements. The cold component of the time-integrated hard x-ray spectrum (E_1, T_1) is correlated with the SRS observed in the time-resolved backscattering diagnostics on the inner-cone laser beams [27]. The corresponding electrons are then sourced in the He gas fill at 10–15% of critical density, consistent with the measured SRS spectrum in the 500–600 nm range and with a temporal dependence following the measured SRS power, i.e., mostly flat during laser peak power. The hot component (E_2, T_2) is likely related to SRS [18,19] and two-plasmon decay [8] around quarter-critical density. Based on time-resolved hard x-ray and SRS measurements, these electrons are accelerated in the last nanosecond of the fourth pulse and sourced accordingly in the simulations, where the laser beams encounter quarter-critical density.

Figure 5 shows a comparison of synthetic and measured hard x-ray images (time-integrated). (a) The first column corresponds to the bremsstrahlung emission from energetic electrons, sourced as described above, plus the calculated plasma thermal emission. The latter contributes less than 10% for the 46 keV image and is negligible for the 115 keV image. (b) The experimental images are shown using the same absolute gray scale, demonstrating the excellent quantitative agreement with the simulations. While the polar view at 115 keV shows x-ray emission that is dominated by the conversion of hot electrons into the Au wall (limb-brightened) and the end cap, the equatorial view at 46 keV is more representative of the low temperature component (E_1, T_1) which converts into the Au plasma expanding from the hohlraum wall where laser beams deposit their energy. While the limb-brightened outer laser cone feature is reproduced very well, individual inner beam spots are missing in the simulations due to their 2D symmetry. Simulations predict 350 J of electrons with energies >100 keV stopping in CH plasma within a radius of 900 μm, which compares well to our experimental measurement of 570 J, hence validating Eq. (1) as a good approximation for quantifying hot electrons from measured hard x-ray emission. Furthermore, simulations show that less than 10% of the signal comes from stopping in the He gas fill along the line of sight of the polar imager and that stopping in Au blowoff is negligible.

In summary, imaging of hard x-ray (> 100 keV) bremsstrahlung emission from a compressing CH capsule in an ignition-scale hohlraum provides an estimate of preheat by energetic electrons generated by laser-plasma interaction. We measure an upper limit of 570 ± 250 J of energetic electrons absorbed in the capsule ablator towards the end of the laser pulse, which translates to a 3.5% increase in adiabat for current NIC cryogenic DT implosions. Integrated radiative-hydrodynamics simulations, including energetic electrons generated by LPI, compare well with these results.

This work was performed under the auspices of the U.S. Department of Energy by the Lawrence Livermore National Laboratory under Contract No. DE-AC52-07NA27344.

[1] J. D. Lindl, P. Amendt, and R. L. Berger *et al.*, Phys. Plasmas **11**, 339 (2004).
[2] R. L. McCrory, D. D. Meyerhofer, and R. Betti *et al.*, Phys. Plasmas **15**, 055503 (2008).
[3] K. A. Tanaka, T. Yamanaka, and K. Nishihara *et al.*, Phys. Plasmas **2**, 2495 (1995).
[4] S. H. Glenzer, B. J. MacGowan, and N. B. Meezan *et al.*, Phys. Rev. Lett. **106**, 085004 (2011).
[5] J. D. Lindl and E. I. Moses, Phys. Plasmas **18**, 050901 (2011).
[6] B. Yaakobi, I. Pelah, and J. Hoose, Phys. Rev. Lett. **37**, 836 (1976).
[7] V. A. Smalyuk, D. Shvarts, and R. Betti *et al.*, Phys. Rev. Lett. **100**, 185005 (2008).

[8] S. P. Regan, N. B. Meezan, and L. J. Suter *et al.*, Phys. Plasmas **17**, 020703 (2010).
[9] S. H. Glenzer, F. B. Rosmej, and R. W. Lee *et al.*, Phys. Rev. Lett. **81**, 365 (1998).
[10] K. A. Brueckner, Phys. Rev. Lett. **36**, 677 (1976).
[11] R. P. Drake, R. E. Turner, and B. F. Lasinski *et al.*, Phys. Rev. A **40**, 3219 (1989).
[12] C. A. Thomas, Phys. Rev. E **81**, 036413 (2010).
[13] S. W. Haan, J. D. Lindl, and D. A. Callahan *et al.*, Phys. Plasmas **18**, 051001 (2011).
[14] G. A. Kyrala, J. L. Kline, and S. Dixit *et al.*, Phys. Plasmas **18**, 056307 (2011).
[15] B. R. Maddox, H. S. Park, and B. A. Remington *et al.*, Rev. Sci. Instrum. **82**, 023111 (2011).
[16] M. B. Schneider, O. S. Jones, and N. B. Meezan *et al.*, Rev. Sci. Instrum. **81**, 10E538 (2010).
[17] J. W. McDonald, R. L. Kauffman, and J. R. Celeste *et al.*, Rev. Sci. Instrum. **75**, 3753 (2004); E. L. Dewald, C. A. Thomas, and S. Hunter *et al.*, *ibid.* **81**, 10D938 (2010).
[18] A. A. Offenberger, R. Fedosejevs, W. Tighe, and W. Rozmus, Phys. Rev. Lett. **49**, 371 (1982).
[19] J. W. Shearer, C. E. Violet, and J. E. Swain *et al.*, Phys. Rev. A **6**, 764 (1972).
[20] J. D. Lindl Phys. Plasmas **2**, 3933 (1995).
[21] D. Mosher, Phys. Fluids **18**, 846 (1975); D. S. Kershaw, Lawrence Livermore National Laboratory Report No. UCRL-77047, 1975.
[22] G. B. Zimmerman and W. L. Kruer, Comments Plasma Phys. Control. Fusion **2**, 85 (1975).
[23] A. A. Solodov and R. Betti, Phys. Plasmas **15**, 042707 (2008); ICRU Report No. 37, 1984.
[24] J. A. Halbleib, R. P. Kensek, and G. D. Valdez *et al.*, IEEE Trans. Nucl. Sci. **39**, 1025 (1992).
[25] I. J. Feng and R. H. Pratt, University of Pittsburgh Report No. PITT-266, 1981.
[26] J. D. Moody, P. Datte, and K. Krauter *et al.*, Rev. Sci. Instrum. **81**, 10D921 (2010).
[27] P. Michel, L. Divol, and R. P. J. Town *et al.*, Phys. Rev. E **83**, 046409 (2011).